PROCEEDINGS OF SCIENCE

Investigations of a Novel Energy Estimator Using Deep Learning for the Surface Detector of the Pierre Auger Observatory

Fiona Ellwanger[a,*] **for the Pierre Auger Collaboration**[b]

[a] *Karlsruhe Institute of Technology, Institute for Astroparticle Physics, Karlsruhe, Germany*
[b] *Observatorio Pierre Auger, Av. San Martín Norte 304, 5613 Malargüe, Argentina*
Full author list: https://www.auger.org/archive/authors_icrc_2023.html

E-mail: spokespersons@auger.org

Exploring physics at energies beyond the reach of human-built accelerators by studying cosmic rays requires an accurate reconstruction of their energy. At the highest energies, cosmic rays are indirectly measured by observing a shower of secondary particles produced by their interaction in the atmosphere. At the Pierre Auger Observatory, the energy of the primary particle is either reconstructed from measurements of the emitted fluorescence light, produced when secondary particles travel through the atmosphere, or shower particles detected with the surface detector at the ground. The surface detector comprises a triangular grid of water-Cherenkov detectors that measure the shower footprint at the ground level. With deep learning, large simulation data sets can be used to train neural networks for reconstruction purposes.

In this work, we present an application of a neural network to estimate the energy of the primary particle from the surface detector data by exploiting the time structure of the particle footprint. When evaluating the precision of the method on air shower simulations, we find the potential to significantly reduce the composition bias compared to methods based on fitting the lateral signal distribution. Furthermore, we investigate possible biases arising from systematic differences between simulations and data.

The 38th International Cosmic Ray Conference (ICRC2023)
26 July – 3 August, 2023
Nagoya, Japan

*Speaker

PoS(ICRC2023)275

1. Introduction

The Pierre Auger Observatory is at this time the largest cosmic ray detector of its kind. It is designed to measure showers of secondary particles produced by cosmic rays interacting in the atmosphere. During clear moonless nights, 24 fluorescence telescopes (FD) observe the longitudinal development of the electromagnetic component of air showers allowing for a calorimetric energy estimate of the primary particle [1]. Additionally, 1600 water-Cherenkov detectors forming the surface detector (SD) measure the signal deposited by incident particles with almost 100% duty cycle [1]. The integrated signal expected at a detector at 1000 m from the impact point of the shower core is strongly correlated to the energy of the primary cosmic ray particle [3, 4]. However, the shape of the time traces in different SD stations, which is not used with standard methods, may contain useful information to improve energy reconstruction. Neural networks (NN) comprise a method to extract this information from the time traces efficiently.

1.1 The reference energy estimator

As a reference model, an analytical method mimicking the current standard method of energy reconstruction [2] is applied for the Monte Carlo test data set. As explained in Refs. [3, 4], the shower size $S(1000)$ is derived from a fit of the signal as a function of the distance to the shower core with a lateral distribution function. Afterwards, the direct energy calibration (DEC) can be performed,

$$\lg(E/\mathrm{eV}) = A + B[\lg(S(1000)/\mathrm{VEM}) - \lg f_{\mathrm{att}}(x)], \tag{1}$$

where $f_{\mathrm{att}}(x) = 1 + a\,x + b\,x^2 + c\,x^3$ describes the attenuation of the shower particles as a function of $x = \sin^2\theta - \sin^2(38°)$ with the zenith angle θ of the shower, and A and B are the calibration parameters at the reference zenith angle of 38° to the Monte Carlo energy.

1.2 The training of the neural network

The showers used for the training of the network were simulated with Corsika [5], using Epos-LHC [6] as hadronic interaction model. The detector response was simulated with the Offline software [7] based on Geant4 [8]. The energy of the ~580 000 showers used for the training ranges from 10^{18} to $10^{20.2}$ eV, following a spectral index of −1. The zenith angle ranges from 0 to 65° and follows a uniform distribution in $\sin^2\theta$. This distribution is expected above the atmosphere for an isotropic flux of primaries. For the mass composition, a uniform mixture of proton, helium, oxygen, and iron is chosen. About 16% of these showers provide an independent test data set. On the station level, the time traces for the triggered PMT, as well as trigger time information, is available for each event. Each of the detectors is equipped with three photomultiplier tubes (PMT). The average trace for the triggered PMTs of one detector station is computed. The first 120 time bins (1 time-bin = 25 ns) [1] after the start bin defined in the trigger algorithm are provided as input for the NN. This trace is given in a logarithmic form, $\tilde{S}(t) = \lg(S(t)/\mathrm{VEM}+1)/\lg(100+1)$. So that non-triggered stations are provided with zeros only. Three convolutional layers are applied until each of the traces is compressed down to 10 features. These 10 features of a station are concatenated with $\tau_{\mathrm{hot},i} = (t_{\mathrm{hot}} - t_i)/\sigma_{\Delta t}$, where t_i is the trigger time of station i, t_{hot} is the trigger time of the

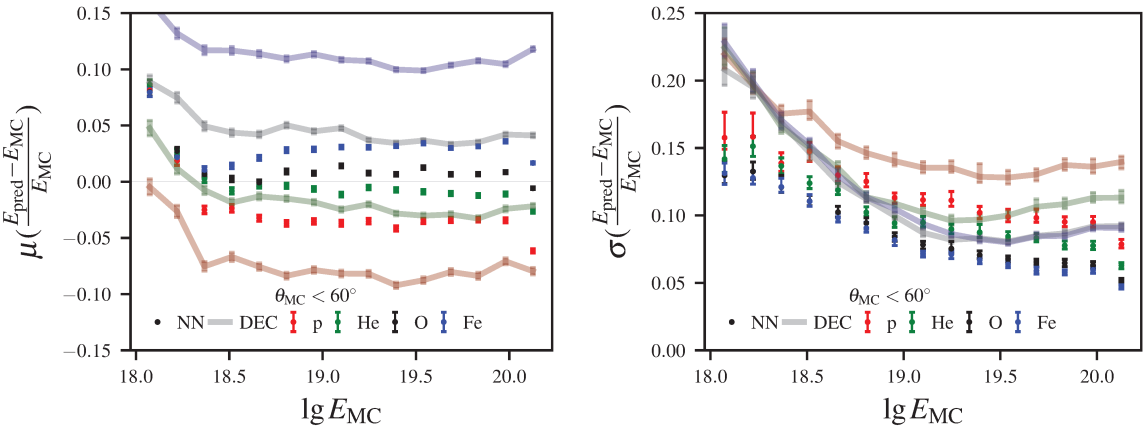

Figure 1: Bias μ, and resolution σ of the NN predictions as a function of energy $\lg(E_{\text{MC}}/\text{eV})$. The four different primary particles proton (p), helium (He), oxygen (O), and iron (Fe) are plotted. Only showers with zenith angles below 60° are considered. For comparison, bias and resolution is also shown for the reference energy estimator, the direct energy calibration (DEC).

station with the highest signal, and $\sigma_{\Delta t}$ is the standard deviation of the time differences $t_{\text{hot}} - t_i$ for the simulated set of showers. The spatial distribution of these 11 features is processed by five separable two-dimensional convolutional layers.

Since the detectors of the SD are placed on a triangular grid, the network has to be provided with this symmetry. Following the approach of Ref. [9], the triangular grid is transformed into a rectangular grid. That way, each shower footprint is rotated and reflected in a pre-defined azimuth range of 30° by twelve unique transformations of the triangular grid. The network is provided with a grid of 5×5 stations, the station with the highest signal being the central one. Since this transformation changes the neighborhood of grid positions, the 3×3 kernel used for the spatial convolution is constrained to be zero for positions that are not actually one of the six neighbors of its center. Finally, the output of the last convolutional layer is flattened, and a densely connected layer produces the network output μ and σ describing the Gaussian probability density function (PDF) of the prediction. The neural network is trained to predict the label $y = \lg(E_{\text{MC}}/\text{eV}) - 19.35$, as it is beneficial for the target values to lie between 1 and −1. The loss function is the negative log-likelihood of the probability the true energy was chosen from the predicted Gaussian PDF described by μ and σ,

$$\text{Loss}_{\text{MDN}}(y; \mu_{\text{pred}}, \sigma_{\text{pred}}) = \lg(\sigma_{\text{pred}}) + \frac{1}{2}\lg(2\pi) + \frac{(y-\mu_{\text{pred}})^2}{2\,\sigma_{\text{pred}}^2}. \tag{2}$$

The optimization is performed by the Adam algorithm [10] with a learning rate of 0.0015, $\beta_1 = 0.9$, and $\beta_2 = 0.999$. During the training, the `EarlyStopping` and `ReduceLROnPlateau` callbacks, available in the TensorFlow framework [11], supervise the training additionally. The training procedure is done 10 times, and the network with the best validation loss is selected. This network was trained for 53 epochs. In Fig. 1, the bias and resolution are shown for the selected network. It can be seen that the mass-dependent bias between proton and iron primaries is reduced from about ±10% for the DEC to ±4% for the NN, while also an improved resolution is obtained with the NN.

2. Performance on measured events

For a set of hybrid events that are successfully reconstructed with SD and FD, the NN prediction can be compared to the calorimetric energy estimate E_{FD} from the FD. Only showers within the range of full SD efficiency [1] (i.e. with $E_{\mathrm{FD}} > 10^{18.5}$ eV) are considered. The data set consists of 3879 events collected between 2005 and 2022. Due to systematic differences between MC simulations and data, like detector aging and muon deficit, the predictions are expected to be biased.

2.1 Detector aging

In contrast to simulations, the response of actual detectors suffers from aging effects, which are effectively described by a change of the so-called *area-over-peak* variable A/P [12] over time. The A/P is given by the ratio of the deposited charge over the peak signal a vertical muon on average produces in the detector. The two values are obtained either with online calibration, performed by station software, or with an offline calibration procedure where calibration histograms are fitted [1]. As shown in Fig. 2, there is a long-term drift of A/P values observed in the detectors, which is mostly attributed to the decrease of the reflectivity of the inner side of the liner (i.e. the plastic bag that holds the water volume of the water-Cherenkov detector) or a change in the absorption length of photons in the water [12]. A change in A/P results in a change of the shape of the signal traces and, thus, affects the predictions of the NNs in contrast to the standard reconstruction where integrated signals are considered. The current Monte Carlo simulation setup, used for generating the training data set, gives us a constant area-over-peak of $(A/P)^{\mathrm{MC}} = 3.2$.

After a number of photons is produced in a water-Cherenkov detector, it approximately evolves according to an exponential decay. The wavelength-dependent decay time τ is related to the detector properties as

$$\frac{1}{\tau(\lambda)} = \frac{c}{n(\lambda)} \left(\frac{1}{L(\lambda)} + [1 - R(\lambda)] \frac{A_{\mathrm{WCD}}}{4 V_{\mathrm{WCD}}} \right), \tag{3}$$

where λ is the wavelength of the photon, $n(\lambda) \approx 1.33$ is the water refraction index, c is the speed of light, $L(\lambda)$ is the absorption length in water, $R(\lambda)$ is the reflectivity of the liner, A_{WCD} is the inner area of the detector, and V_{WCD} the water volume in the detector. The depth of the water volume is $h = 1.2\,\mathrm{m}$ and the radius of the water cylinder $r = 1.8\,\mathrm{m}$ [1]. Using an effective absorption length of $L \approx 100\,\mathrm{m}$ and reflectivity $R = 0.94$ over the whole wavelength range λ, we obtain values around $\tau = 86\,\mathrm{ns}$ for the decay time. Note that the detector response in time t is approximated with a truncated exponential decay

$$D_\alpha(t) = \tfrac{1}{\alpha} \exp\left(-\tfrac{t}{\alpha}\right) \Theta(t). \tag{4}$$

where α is the decay constant and $\Theta(t)$ is the Heaviside step function. The signal measured by a detector is given by a convolution of the distribution of arriving particles $p(t)$ with the detector response $D_\alpha(t)$. For example, for a single arriving particle at $t = t_1$, we have $p(t) = \delta(t - t_1)$ and, thus, its measured signal is given by

$$S_\alpha(t) = \tfrac{S_1}{\alpha} \exp\left(-\tfrac{t-t_1}{\alpha}\right) \Theta(t - t_1), \tag{5}$$

where S_1 is the signal deposited by one particle. We can define the *area* A and the *peak* P of the resulting signal as,

$$A\,\Delta t = \int_{-\infty}^{\infty} S_\alpha(t)\,\mathrm{d}t = \int_{-\infty}^{\infty} \tfrac{S_1}{\alpha} \exp\left(-\tfrac{t}{\alpha}\right)\,\Theta(t)\,\mathrm{d}t \equiv S_1, \quad \text{and} \quad P = S_\alpha(t{=}t_1) = \frac{S_1}{\alpha}, \tag{6}$$

where $\Delta t = 25\,\mathrm{ns}$ is the sampling frequency of the ADC. From this definition we see that the A/P is simply related to the decay time of the detector response in Eq. (4), i.e. $A/P = \alpha/\Delta t$. The equivalent area-over-peak for a decay time of $\tau = 86\,\mathrm{ns}$ is therefore, $A/P = \tau/\Delta t \approx 3.4$. In Fourier space, the detected signal can be simply written as the product, $\tilde{S}_\alpha(\omega) = \tilde{p}(\omega)\,\tilde{D}_\alpha(\omega)$, where ω is the angular frequency. For modeling the long-term performance we can change the signal $S_\alpha(t)$ measured with a detector response $D_\alpha(t)$ to the signal that would have been observed with another decay constant β, which is particularly simple with Fourier transforms (FT),

$$\tilde{S}_\beta(\omega) = \tilde{S}_\alpha(\omega)\,\frac{\tilde{D}_\beta(\omega)}{\tilde{D}_\alpha(\omega)} = \tilde{S}_\alpha(\omega)\,\tilde{K}_{\alpha\to\beta}(\omega), \tag{7}$$

where $\tilde{K}_{\alpha\to\beta}(\omega)$ is the FT of the convolutional kernel $K(t)_{\alpha\to\beta}$. The FT of the detector response $D_\alpha(t)$ is given by $\tilde{D}_\alpha(\omega) = \mathrm{i}/(\mathrm{i}-\alpha\omega)$. Therefore, the time-domain kernel for partial de/convolution from response with decay time α to decay time β is given by

$$K_{\alpha\to\beta}(t) = \int_{-\infty}^{\infty} \tilde{K}_{\alpha\to\beta}(\omega)\,e^{\mathrm{i}\omega t}\,\mathrm{d}\omega = \int_{-\infty}^{\infty} \frac{\tilde{D}_\beta}{\tilde{D}_\alpha}\,e^{\mathrm{i}\omega t}\,\mathrm{d}\omega = r\,\delta(t) + (1-r)D_\beta(t), \tag{8}$$

where $r = \alpha/\beta$ is the ratio of the decay times or the respective area-over-peak ratios. We can immediately observe two useful properties of this kernel: (a) a trace remains unchanged when the kernel is applied with $\alpha \equiv \beta$, and (b) the kernel does not change the integral of a trace (since both δ and D_β preserve the norm), and, thus, the kernel does not change the total signal. Furthermore, examining the structure of the kernel, the first term produces a copy of a trace scaled by a factor r while the second term is partially convolving or deconvolving a trace with weight $1-r$ when $\beta > \alpha$ or $\beta < \alpha$, respectively. From an original signal trace $S(t)$ with a given area-over-peak A/P and $\alpha = A/P\,\Delta t$, an aging-corrected trace $S'(t)$ with the nominal area-over-peak $(A/P)^{\mathrm{MC}} = 3.2$ value and $\beta = (A/P)^{\mathrm{MC}}\,\Delta t$ is produced with the following folding integral

$$S'(t) = \left(S * K_{\alpha\to\beta}\right)(t) = \int_{-\infty}^{\infty} K_{\alpha\to\beta}(t')\,S(t-t')\,\mathrm{d}t'. \tag{9}$$

In Fig. 2, an example for the partial de/convolution of a time trace is shown. As in most cases, the difference in A/P is quite small, the difference between the original and the partially de/convolved traces is only barely visible. However, for saturated traces the flat plateau is not reproduced. Therefore, for future analysis the partial de/convolution will be changed so that the trace is not changed where it is saturated.

The NN prediction of the primary energy on measured data shows a bias dependent on the average area-over-peak $\langle A/P\rangle$ of the triggered stations in the respective events, which is undesirable in an optimal estimator of energy. When the partial de/convolution of the traces is performed according to Eq. (9), the $\langle A/P\rangle$ dependence of the bias is almost removed (see Fig. 3). However, a global bias of the order of 5% is observed and needs to be corrected. After the bias correction discussed in the following section is performed, the additional partial de/convolution of the input traces leads to an improvement of the resolution of the corrected predictions of ∼0.7% above $10^{18.5}\,\mathrm{eV}$.

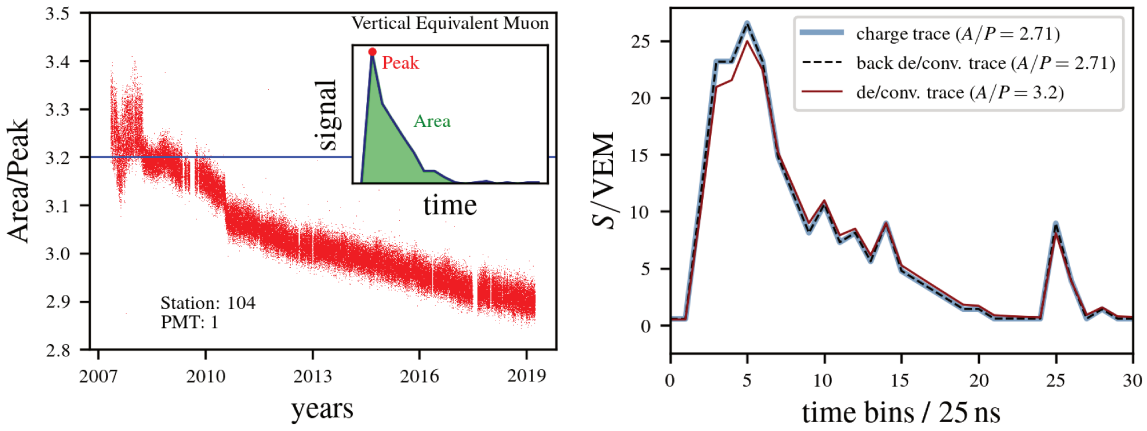

Figure 2: *Left:* A typical long-term evolution of the area-over-peak A/P for one PMT of a randomly chosen station (104, in this case) obtained from the Auger monitoring system. The blue line denotes the current value of $(A/P)^{\mathrm{MC}} = 3.2$ in simulations. *Right:* Typical cases for partial de/convolution. The blue line (underneath the black dashed line) represents the original trace, while the red curve corresponds to the partially de/convolved trace that should match the $(A/P)^{\mathrm{MC}} = 3.2$ of Monte Carlo simulations. Partially de/convolving the transformed trace back to the original A/P results in the black dashed line.

2.2 Bias correction

The models used to simulate ultra-high-energy particle showers do not fully reproduce the measurements. In fact, more muons are observed in measurements than are predicted by hadronic interaction models [13]. As the algorithm developed by the NN is very complex, it is hard to predict the effect of such mismatches between training data and measured events on the predictions. First, it is observed that the energy is, on average, overestimated. It is suspected that an increase in the number of muons produced in the shower leads to more particles reaching the ground, causing higher signals at the stations. Moreover, a zenith-dependent bias is observed. Understanding the cause of this bias is still a work in progress. Nevertheless, correcting for it on average is possible by fitting a linear calibration function f_{cal} in $\sec\theta$ to the energy bias observed in the hybrid data set using the least-squared method. In Fig. 3, the bias for the NN on hybrid data is shown together with the calibration fit. Please note that the calibrated prediction $E^{\mathrm{cal}}_{\mathrm{pred}} = E_{\mathrm{pred}}/[f_{\mathrm{cal}}(\sec\theta) + 1]$ is, on average unbiased with respect to E_{FD}, as the calibration function contains not only the zenith dependence but also a constant offset. With the bias correction the resolution of the predictions is reduced by ~2% for events above $10^{18.5}$ eV.

In Fig. 4, the performance for the corrected predictions is shown. It is observed that bias and resolution are competitive with the standard reconstruction. However, the superiority of the NN (see Fig. 1) is lost. This is due to different reasons, such as additional systematic differences between simulations and measurements, which are all a subject of further investigations. Moreover, as the energy in the standard reconstruction is calibrated to the hybrid data set, no effects from the mass-dependent bias are expected for a smooth change in the composition. For the NN, however, a composition change with energy will introduce an energy-dependent bias. Nevertheless, for a composition that is changing faster, or at energies where the hybrid data set does not provide enough data, the NN is expected to be less affected due to its mass-dependent bias having only half the

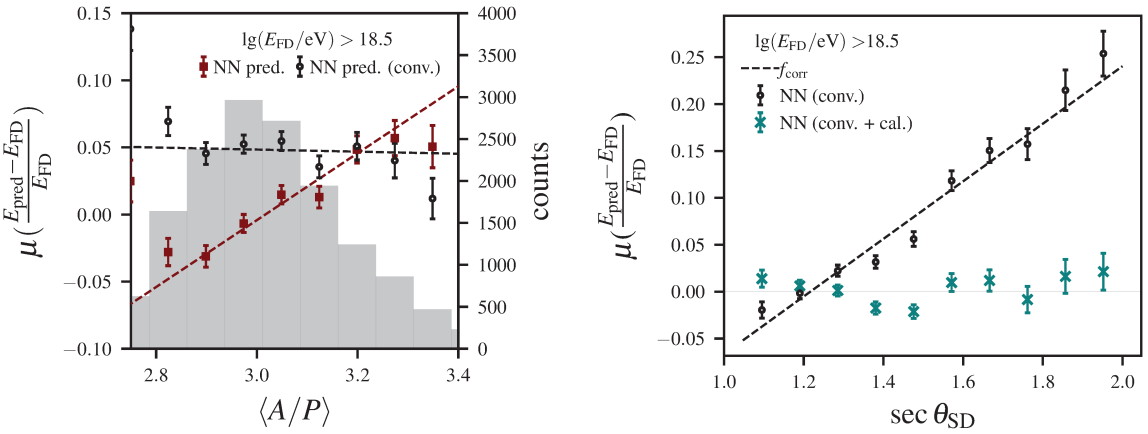

Figure 3: *Left:* Bias μ of the energy E_{pred} predicted by the NN compared to the FD reconstructed energy E_{FD} as a function of the average area-over-peak $\langle A/P \rangle$ of the triggered stations in the respective events. After the partial de/convolution of the measured data traces (black circles), the NN prediction no longer depends on the average A/P of the event. For visualization, linear fits to the relative errors as a function of $\langle A/P \rangle$ in the range ($2.9 < \langle A/P \rangle < 3.2$) are shown (dashed lines). The histogram indicates the distribution of $\langle A/P \rangle$. *Right:* Correction of the zenith-dependent bias μ. The calibration function $f_{\text{cal}}(\sec\theta) = p_1 \sec\theta + p_0$ (dashed line), is derived by a least-squared fit to the relative error with respect to the FD reconstructed energy of the hybrid events. The calibrated predictions are obtained with $E^{\text{cal}}_{\text{pred}} = E_{\text{pred}}/[f_{\text{cal}}(\sec\theta) + 1]$ (green ×).

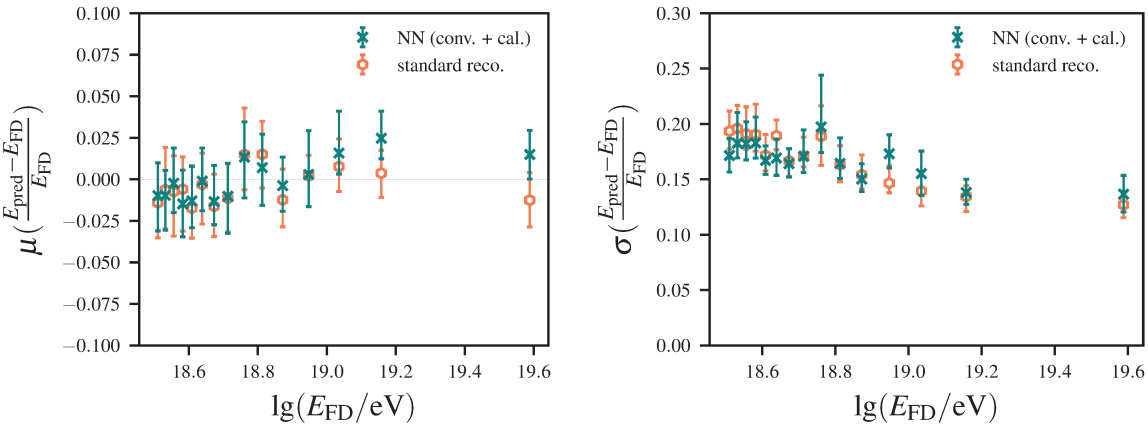

Figure 4: Bias μ, and resolution σ, for NN predictions of showers with reconstructed energy from FD above $10^{18.5}$ eV (green ×). The $\sec\theta$ calibration and the partial de/convolution of the input traces is applied. For comparison, the results of the standard reconstruction are shown (orange hexagons).

magnitude of the standard reconstruction, see Fig. 1.

In Fig. 5, the correlation of the corrected NN predictions with the standard reconstruction for the 273 277 events above $10^{18.4}$ eV collected between 2004 and 2021 with successful reconstruction of the SD data is shown. The same calibration function derived from the hybrid data is used for the bias correction. In general, there is good agreement between the NN prediction and the standard reconstruction. Nevertheless, the observed biases need to be further investigated.

3. Conclusions

We have shown that the NN can extract useful information from the time traces of the surface detector. By exploiting the time structure of the signal, we find the potential to reduce the mass dependency of the energy reconstruction compared to the standard methods. When applied to real operating conditions, using hybrid events, systematic differences between simulations and measured data cause the NN predictions to lose their superiority. Furthermore, the high precision of the standard reconstruction optimized for the observed composition may not leave too much room for improvement in terms of the resolution and bias. Nevertheless, due to the reduced mass-dependent bias, the use of the NN can be beneficial, if a mass composition different from the hybrid data set is considered. To interpret the differences found between the NN predictions and the standard reconstruction, the observed zenith-dependent bias has to be investigated in more detail. Furthermore, we plan to examine the composition dependency of the energy estimators for the measured data using mass-sensitive observables, like the shower maximum X_{max} and the muon content of the shower [14, 15]. Moreover, the scintillator detectors installed as a part of the AugerPrime upgrade [16] will improve the mass separation capabilities on the event-by-event level.

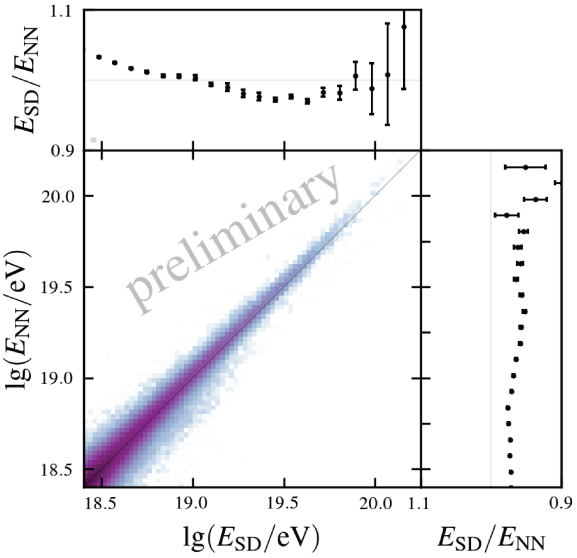

Figure 5: Correlation between corrected NN prediction E_{NN} and energy obtained from the standard reconstruction E_{SD} for events with successful SD reconstruction. The marginal plots show the profile of the ratio of the two energy estimates.

References

[1] A. Aab *et al.* [Pierre Auger], Nucl. Instrum. Meth. A **798** (2015) 172–213.
[2] J. Hersil *et al.*, Phys. Rev. Lett. **6** (1961) 22.
[3] A. Aab *et al.* [Pierre Auger], JINST **15** (2020) 10021.
[4] A. Aab *et al.* [Pierre Auger], Phys. Rev. D **102** (2020) 062005.
[5] D. Heck *et al.*, FZKA **6019** (1998).
[6] T. Pierog *et al.*, Phys. Rev. C **92** (2015) 034906.
[7] S. Argirò *et al.*, Nucl. Instrum. Meth. A **580(3)** (2007) 1485–1496.
[8] S. Agostinelli *et al.*, Nucl. Instrum. Meth. A **506** (2003) 250–303.
[9] S. Hahn *et al.*, Proc. 37th ICRC 2021 Berlin, Germany. **PoS** (2021) 239.
[10] D. Kingma, J. Ba, Proc. 3rd ICLR 2015 San Diego, CA, USA, [1412.6980].
[11] M. Abadi *et al.* [Google Research], [1603.04467].
[12] R. Sato *et al.* [Pierre Auger], Proc. 32th ICRC 2011 Beijing, China. **PoS** (2011) 204.
[13] A. Aab *et al.* [Pierre Auger], Phys. Rev. Lett. **117** (2016) 192001.
[14] A. Aab *et al.* [Pierre Auger], JINST **16** (2021) 07019.
[15] A. Aab *et al.* [Pierre Auger], JINST **16** (2021) 07016.
[16] J. Stasielak *et al.* [Pierre Auger], Int. J. Mod. Phys. A **37** (2022) 2240012.

The Pierre Auger Collaboration

A. Abdul Halim[13], P. Abreu[72], M. Aglietta[54,52], I. Allekotte[1], K. Almeida Cheminant[70], A. Almela[7,12], R. Aloisio[45,46], J. Alvarez-Muñiz[79], J. Ammerman Yebra[79], G.A. Anastasi[54,52], L. Anchordoqui[86], B. Andrada[7], S. Andringa[72], C. Aramo[50], P.R. Araújo Ferreira[42], E. Arnone[63,52], J. C. Arteaga Velázquez[67], H. Asorey[7], P. Assis[72], G. Avila[11], E. Avocone[57,46], A.M. Badescu[75], A. Bakalova[32], A. Balaceanu[73], F. Barbato[45,46], A. Bartz Mocellin[85], J.A. Bellido[13,69], C. Berat[36], M.E. Bertaina[63,52], G. Bhatta[70], M. Bianciotto[63,52], P.L. Biermann[h], V. Binet[5], K. Bismark[39,7], T. Bister[80,81], J. Biteau[37], J. Blazek[32], C. Bleve[36], J. Blümer[41], M. Boháčová[32], D. Boncioli[57,46], C. Bonifazi[8,26], L. Bonneau Arbeletche[21], N. Borodai[70], J. Brack[j], P.G. Brichetto Orchera[7], F.L. Briechle[42], A. Bueno[78], S. Buitink[15], M. Buscemi[47,61], M. Büsken[39,7], A. Bwembya[80,81], K.S. Caballero-Mora[66], S. Cabana-Freire[79], L. Caccianiga[59,49], I. Caracas[38], R. Caruso[58,47], A. Castellina[54,52], F. Catalani[18], G. Cataldi[48], L. Cazon[79], M. Cerda[10], A. Cermenati[45,46], J.A. Chinellato[21], J. Chudoba[32], L. Chytka[33], R.W. Clay[13], A.C. Cobos Cerutti[6], R. Colalillo[60,50], A. Coleman[90], M.R. Coluccia[48], R. Conceição[72], A. Condorelli[37], G. Consolati[49,55], M. Conte[56,48], F. Convenga[41], D. Correia dos Santos[28], P.J. Costa[72], C.E. Covault[84], M. Cristinziani[44], C.S. Cruz Sanchez[3], S. Dasso[4,2], K. Daumiller[41], B.R. Dawson[13], R.M. de Almeida[28], J. de Jesús[7,41], S.J. de Jong[80,81], J.R.T. de Mello Neto[26,27], I. De Mitri[45,46], J. de Oliveira[17], D. de Oliveira Franco[21], F. de Palma[56,48], V. de Souza[19], E. De Vito[56,48], A. Del Popolo[58,47], O. Deligny[34], N. Denner[32], L. Deval[41,7], A. di Matteo[52], M. Dobre[73], C. Dobrigkeit[21], J.C. D'Olivo[68], L.M. Domingues Mendes[72], J.C. dos Anjos, R.C. dos Anjos[25], J. Ebr[32], F. Ellwanger[41], M. Emam[80,81], R. Engel[39,41], I. Epicoco[56,48], M. Erdmann[42], A. Etchegoyen[7,12], C. Evoli[45,46], H. Falcke[80,82,81], J. Farmer[89], G. Farrar[88], A.C. Fauth[21], N. Fazzini[e], F. Feldbusch[40], F. Fenu[41,d], A. Fernandes[72], B. Fick[87], J.M. Figueira[7], A. Filipčič[77,76], T. Fitoussi[41], B. Flaggs[90], T. Fodran[80], T. Fujii[89,f], A. Fuster[7,12], C. Galea[80], C. Galelli[59,49], B. García[6], C. Gaudu[38], H. Gemmeke[40], F. Gesualdi[7,41], A. Gherghel-Lascu[73], P.L. Ghia[34], U. Giaccari[48], M. Giammarchi[49], J. Glombitza[42,g], F. Gobbi[10], F. Gollan[7], G. Golup[1], M. Gómez Berisso[1], P.F. Gómez Vitale[11], J.P. Gongora[11], J.M. González[1], N. González[7], I. Goos[1], D. Góra[70], A. Gorgi[54,52], M. Gottowik[79], T.D. Grubb[13], F. Guarino[60,50], G.P. Guedes[22], E. Guido[44], S. Hahn[39], P. Hamal[32], M.R. Hampel[7], P. Hansen[3], D. Harari[1], V.M. Harvey[13], A. Haungs[41], T. Hebbeker[42], C. Hojvat[e], J.R. Hörandel[80,81], P. Horvath[33], M. Hrabovský[33], T. Huege[41,15], A. Insolia[58,47], P.G. Isar[74], P. Janecek[32], J.A. Johnsen[85], J. Jurysek[32], A. Kääpä[38], K.H. Kampert[38], B. Keilhauer[41], A. Khakurdikar[80], V.V. Kizakke Covilakam[7,41], H.O. Klages[41], M. Kleifges[40], F. Knapp[39], N. Kunka[40], B.L. Lago[16], N. Langner[42], M.A. Leigui de Oliveira[24], Y Lema-Capeans[79], V. Lenok[39], A. Letessier-Selvon[35], I. Lhenry-Yvon[34], D. Lo Presti[58,47], L. Lopes[72], L. Lu[91], Q. Luce[39], J.P. Lundquist[76], A. Machado Payeras[21], M. Majercakova[32], D. Mandat[32], B.C. Manning[13], P. Mantsch[e], S. Marafico[34], F.M. Mariani[59,49], A.G. Mariazzi[3], I.C. Mariş[14], G. Marsella[61,47], D. Martello[56,48], S. Martinelli[41,7], O. Martínez Bravo[64], M.A. Martins[79], M. Mastrodicasa[57,46], H.J. Mathes[41], J. Matthews[a], G. Matthiae[62,51], E. Mayotte[85,38], S. Mayotte[85], P.O. Mazur[e], G. Medina-Tanco[68], J. Meinert[38], D. Melo[7], A. Menshikov[40], C. Merx[41], S. Michal[33], M.I. Micheletti[5], L. Miramonti[59,49], S. Mollerach[1], F. Montanet[36], L. Morejon[38], C. Morello[54,52], A.L. Müller[32], K. Mulrey[80,81], R. Mussa[52], M. Muzio[88], W.M. Namasaka[38], S. Negi[32], L. Nellen[68], K. Nguyen[87], G. Nicora[9], M. Niculescu-Oglinzanu[73], M. Niechciol[44], D. Nitz[87], D. Nosek[31], V. Novotny[31], L. Nožka[33], A Nucita[56,48], L.A. Núñez[30], C. Oliveira[19], M. Palatka[32], J. Pallotta[9], S. Panja[32], G. Parente[79], T. Paulsen[38], J. Pawlowsky[38], M. Pech[32], J. Pękala[70], R. Pelayo[65], L.A.S. Pereira[23], E.E. Pereira Martins[39,7], J. Perez Armand[20], C. Pérez Bertolli[7,41], L. Perrone[56,48], S. Petrera[45,46], C. Petrucci[57,46], T. Pierog[41], M. Pimenta[72], M. Platino[7], B. Pont[80], M. Pothast[81,80], M. Pourmohammad Shahvar[61,47], P. Privitera[89], M. Prouza[32], A. Puyleart[87], S. Querchfeld[38], J. Rautenberg[38], D. Ravignani[7], M. Reininghaus[39], J. Ridky[32], F. Riehn[79], M. Risse[44], V. Rizi[57,46], W. Rodrigues de Carvalho[80], E. Rodriguez[7,41], J. Rodriguez Rojo[11], M.J. Roncoroni[7], S. Rossoni[43], M. Roth[41], E. Roulet[1], A.C. Rovero[4], P. Ruehl[44], A. Saftoiu[73], M. Saharan[80], F. Salamida[57,46], H. Salazar[64], G. Salina[51], J.D. Sanabria Gomez[30], F. Sánchez[7], E.M. Santos[20], E. Santos[32],

F. Sarazin[85], R. Sarmento[72], R. Sato[11], P. Savina[91], C.M. Schäfer[41], V. Scherini[56,48], H. Schieler[41], M. Schimassek[34], M. Schimp[38], F. Schlüter[41], D. Schmidt[39], O. Scholten[15,i], H. Schoorlemmer[80,81], P. Schovánek[32], F.G. Schröder[90,41], J. Schulte[42], T. Schulz[41], S.J. Sciutto[3], M. Scornavacche[7,41], A. Segreto[53,47], S. Sehgal[38], S.U. Shivashankara[76], G. Sigl[43], G. Silli[7], O. Sima[73,b], F. Simon[40], R. Smau[73], R. Šmída[89], P. Sommers[k], J.F. Soriano[86], R. Squartini[10], M. Stadelmaier[32], D. Stanca[73], S. Stanič[76], J. Stasielak[70], P. Stassi[36], S. Strähnz[39], M. Straub[42], M. Suárez-Durán[14], T. Suomijärvi[37], A.D. Supanitsky[7], Z. Svozilikova[32], Z. Szadkowski[71], A. Tapia[29], C. Taricco[63,52], C. Timmermans[81,80], O. Tkachenko[41], P. Tobiska[32], C.J. Todero Peixoto[18], B. Tomé[72], Z. Torrès[36], A. Travaini[10], P. Travnicek[32], C. Trimarelli[57,46], M. Tueros[3], M. Unger[41], L. Vaclavek[33], M. Vacula[33], J.F. Valdés Galicia[68], L. Valore[60,50], E. Varela[64], A. Vásquez-Ramírez[30], D. Veberič[41], C. Ventura[27], I.D. Vergara Quispe[3], V. Verzi[51], J. Vicha[32], J. Vink[83], J. Vlastimil[32], S. Vorobiov[76], C. Watanabe[26], A.A. Watson[c], A. Weindl[41], L. Wiencke[85], H. Wilczyński[70], D. Wittkowski[38], B. Wundheiler[7], B. Yue[38], A. Yushkov[32], O. Zapparrata[14], E. Zas[79], D. Zavrtanik[76,77], M. Zavrtanik[77,76]

[1] Centro Atómico Bariloche and Instituto Balseiro (CNEA-UNCuyo-CONICET), San Carlos de Bariloche, Argentina
[2] Departamento de Física and Departamento de Ciencias de la Atmósfera y los Océanos, FCEyN, Universidad de Buenos Aires and CONICET, Buenos Aires, Argentina
[3] IFLP, Universidad Nacional de La Plata and CONICET, La Plata, Argentina
[4] Instituto de Astronomía y Física del Espacio (IAFE, CONICET-UBA), Buenos Aires, Argentina
[5] Instituto de Física de Rosario (IFIR) – CONICET/U.N.R. and Facultad de Ciencias Bioquímicas y Farmacéuticas U.N.R., Rosario, Argentina
[6] Instituto de Tecnologías en Detección y Astropartículas (CNEA, CONICET, UNSAM), and Universidad Tecnológica Nacional – Facultad Regional Mendoza (CONICET/CNEA), Mendoza, Argentina
[7] Instituto de Tecnologías en Detección y Astropartículas (CNEA, CONICET, UNSAM), Buenos Aires, Argentina
[8] International Center of Advanced Studies and Instituto de Ciencias Físicas, ECyT-UNSAM and CONICET, Campus Miguelete – San Martín, Buenos Aires, Argentina
[9] Laboratorio Atmósfera – Departamento de Investigaciones en Láseres y sus Aplicaciones – UNIDEF (CITEDEF-CONICET), Argentina
[10] Observatorio Pierre Auger, Malargüe, Argentina
[11] Observatorio Pierre Auger and Comisión Nacional de Energía Atómica, Malargüe, Argentina
[12] Universidad Tecnológica Nacional – Facultad Regional Buenos Aires, Buenos Aires, Argentina
[13] University of Adelaide, Adelaide, S.A., Australia
[14] Université Libre de Bruxelles (ULB), Brussels, Belgium
[15] Vrije Universiteit Brussels, Brussels, Belgium
[16] Centro Federal de Educação Tecnológica Celso Suckow da Fonseca, Petropolis, Brazil
[17] Instituto Federal de Educação, Ciência e Tecnologia do Rio de Janeiro (IFRJ), Brazil
[18] Universidade de São Paulo, Escola de Engenharia de Lorena, Lorena, SP, Brazil
[19] Universidade de São Paulo, Instituto de Física de São Carlos, São Carlos, SP, Brazil
[20] Universidade de São Paulo, Instituto de Física, São Paulo, SP, Brazil
[21] Universidade Estadual de Campinas, IFGW, Campinas, SP, Brazil
[22] Universidade Estadual de Feira de Santana, Feira de Santana, Brazil
[23] Universidade Federal de Campina Grande, Centro de Ciencias e Tecnologia, Campina Grande, Brazil
[24] Universidade Federal do ABC, Santo André, SP, Brazil
[25] Universidade Federal do Paraná, Setor Palotina, Palotina, Brazil
[26] Universidade Federal do Rio de Janeiro, Instituto de Física, Rio de Janeiro, RJ, Brazil
[27] Universidade Federal do Rio de Janeiro (UFRJ), Observatório do Valongo, Rio de Janeiro, RJ, Brazil
[28] Universidade Federal Fluminense, EEIMVR, Volta Redonda, RJ, Brazil
[29] Universidad de Medellín, Medellín, Colombia
[30] Universidad Industrial de Santander, Bucaramanga, Colombia

PoS(ICRC2023)275

[31] Charles University, Faculty of Mathematics and Physics, Institute of Particle and Nuclear Physics, Prague, Czech Republic
[32] Institute of Physics of the Czech Academy of Sciences, Prague, Czech Republic
[33] Palacky University, Olomouc, Czech Republic
[34] CNRS/IN2P3, IJCLab, Université Paris-Saclay, Orsay, France
[35] Laboratoire de Physique Nucléaire et de Hautes Energies (LPNHE), Sorbonne Université, Université de Paris, CNRS-IN2P3, Paris, France
[36] Univ. Grenoble Alpes, CNRS, Grenoble Institute of Engineering Univ. Grenoble Alpes, LPSC-IN2P3, 38000 Grenoble, France
[37] Université Paris-Saclay, CNRS/IN2P3, IJCLab, Orsay, France
[38] Bergische Universität Wuppertal, Department of Physics, Wuppertal, Germany
[39] Karlsruhe Institute of Technology (KIT), Institute for Experimental Particle Physics, Karlsruhe, Germany
[40] Karlsruhe Institute of Technology (KIT), Institut für Prozessdatenverarbeitung und Elektronik, Karlsruhe, Germany
[41] Karlsruhe Institute of Technology (KIT), Institute for Astroparticle Physics, Karlsruhe, Germany
[42] RWTH Aachen University, III. Physikalisches Institut A, Aachen, Germany
[43] Universität Hamburg, II. Institut für Theoretische Physik, Hamburg, Germany
[44] Universität Siegen, Department Physik – Experimentelle Teilchenphysik, Siegen, Germany
[45] Gran Sasso Science Institute, L'Aquila, Italy
[46] INFN Laboratori Nazionali del Gran Sasso, Assergi (L'Aquila), Italy
[47] INFN, Sezione di Catania, Catania, Italy
[48] INFN, Sezione di Lecce, Lecce, Italy
[49] INFN, Sezione di Milano, Milano, Italy
[50] INFN, Sezione di Napoli, Napoli, Italy
[51] INFN, Sezione di Roma "Tor Vergata", Roma, Italy
[52] INFN, Sezione di Torino, Torino, Italy
[53] Istituto di Astrofisica Spaziale e Fisica Cosmica di Palermo (INAF), Palermo, Italy
[54] Osservatorio Astrofisico di Torino (INAF), Torino, Italy
[55] Politecnico di Milano, Dipartimento di Scienze e Tecnologie Aerospaziali , Milano, Italy
[56] Università del Salento, Dipartimento di Matematica e Fisica "E. De Giorgi", Lecce, Italy
[57] Università dell'Aquila, Dipartimento di Scienze Fisiche e Chimiche, L'Aquila, Italy
[58] Università di Catania, Dipartimento di Fisica e Astronomia "Ettore Majorana", Catania, Italy
[59] Università di Milano, Dipartimento di Fisica, Milano, Italy
[60] Università di Napoli "Federico II", Dipartimento di Fisica "Ettore Pancini", Napoli, Italy
[61] Università di Palermo, Dipartimento di Fisica e Chimica "E. Segrè", Palermo, Italy
[62] Università di Roma "Tor Vergata", Dipartimento di Fisica, Roma, Italy
[63] Università Torino, Dipartimento di Fisica, Torino, Italy
[64] Benemérita Universidad Autónoma de Puebla, Puebla, México
[65] Unidad Profesional Interdisciplinaria en Ingeniería y Tecnologías Avanzadas del Instituto Politécnico Nacional (UPIITA-IPN), México, D.F., México
[66] Universidad Autónoma de Chiapas, Tuxtla Gutiérrez, Chiapas, México
[67] Universidad Michoacana de San Nicolás de Hidalgo, Morelia, Michoacán, México
[68] Universidad Nacional Autónoma de México, México, D.F., México
[69] Universidad Nacional de San Agustin de Arequipa, Facultad de Ciencias Naturales y Formales, Arequipa, Peru
[70] Institute of Nuclear Physics PAN, Krakow, Poland
[71] University of Łódź, Faculty of High-Energy Astrophysics,Łódź, Poland
[72] Laboratório de Instrumentação e Física Experimental de Partículas – LIP and Instituto Superior Técnico – IST, Universidade de Lisboa – UL, Lisboa, Portugal
[73] "Horia Hulubei" National Institute for Physics and Nuclear Engineering, Bucharest-Magurele, Romania
[74] Institute of Space Science, Bucharest-Magurele, Romania
[75] University Politehnica of Bucharest, Bucharest, Romania
[76] Center for Astrophysics and Cosmology (CAC), University of Nova Gorica, Nova Gorica, Slovenia
[77] Experimental Particle Physics Department, J. Stefan Institute, Ljubljana, Slovenia

PoS(ICRC2023)275

[78] Universidad de Granada and C.A.F.P.E., Granada, Spain
[79] Instituto Galego de Física de Altas Enerxías (IGFAE), Universidade de Santiago de Compostela, Santiago de Compostela, Spain
[80] IMAPP, Radboud University Nijmegen, Nijmegen, The Netherlands
[81] Nationaal Instituut voor Kernfysica en Hoge Energie Fysica (NIKHEF), Science Park, Amsterdam, The Netherlands
[82] Stichting Astronomisch Onderzoek in Nederland (ASTRON), Dwingeloo, The Netherlands
[83] Universiteit van Amsterdam, Faculty of Science, Amsterdam, The Netherlands
[84] Case Western Reserve University, Cleveland, OH, USA
[85] Colorado School of Mines, Golden, CO, USA
[86] Department of Physics and Astronomy, Lehman College, City University of New York, Bronx, NY, USA
[87] Michigan Technological University, Houghton, MI, USA
[88] New York University, New York, NY, USA
[89] University of Chicago, Enrico Fermi Institute, Chicago, IL, USA
[90] University of Delaware, Department of Physics and Astronomy, Bartol Research Institute, Newark, DE, USA
[91] University of Wisconsin-Madison, Department of Physics and WIPAC, Madison, WI, USA

—

[a] Louisiana State University, Baton Rouge, LA, USA
[b] also at University of Bucharest, Physics Department, Bucharest, Romania
[c] School of Physics and Astronomy, University of Leeds, Leeds, United Kingdom
[d] now at Agenzia Spaziale Italiana (ASI). Via del Politecnico 00133, Roma, Italy
[e] Fermi National Accelerator Laboratory, Fermilab, Batavia, IL, USA
[f] now at Graduate School of Science, Osaka Metropolitan University, Osaka, Japan
[g] now at ECAP, Erlangen, Germany
[h] Max-Planck-Institut für Radioastronomie, Bonn, Germany
[i] also at Kapteyn Institute, University of Groningen, Groningen, The Netherlands
[j] Colorado State University, Fort Collins, CO, USA
[k] Pennsylvania State University, University Park, PA, USA

Acknowledgments

The successful installation, commissioning, and operation of the Pierre Auger Observatory would not have been possible without the strong commitment and effort from the technical and administrative staff in Malargüe. We are very grateful to the following agencies and organizations for financial support:

Argentina – Comisión Nacional de Energía Atómica; Agencia Nacional de Promoción Científica y Tecnológica (ANPCyT); Consejo Nacional de Investigaciones Científicas y Técnicas (CONICET); Gobierno de la Provincia de Mendoza; Municipalidad de Malargüe; NDM Holdings and Valle Las Leñas; in gratitude for their continuing cooperation over land access; Australia – the Australian Research Council; Belgium – Fonds de la Recherche Scientifique (FNRS); Research Foundation Flanders (FWO); Brazil – Conselho Nacional de Desenvolvimento Científico e Tecnológico (CNPq); Financiadora de Estudos e Projetos (FINEP); Fundação de Amparo à Pesquisa do Estado de Rio de Janeiro (FAPERJ); São Paulo Research Foundation (FAPESP) Grants No. 2019/10151-2, No. 2010/07359-6 and No. 1999/05404-3; Ministério da Ciência, Tecnologia, Inovações e Comunicações (MCTIC); Czech Republic – Grant No. MSMT CR LTT18004, LM2015038, LM2018102, CZ.02.1.01/0.0/0.0/16_013/0001402, CZ.02.1.01/0.0/0.0/18_046/0016010 and CZ.02.1.01/0.0/0.0/17_049/0008422; France – Centre de Calcul IN2P3/CNRS; Centre National de la Recherche Scientifique (CNRS); Conseil Régional Ile-de-France; Département Physique Nucléaire et Corpusculaire (PNC-IN2P3/CNRS); Département Sciences de l'Univers (SDU-INSU/CNRS); Institut Lagrange de Paris (ILP) Grant No. LABEX ANR-10-LABX-63 within the Investissements d'Avenir Programme Grant No. ANR-11-IDEX-0004-02; Germany – Bundesministerium für Bildung und Forschung (BMBF); Deutsche Forschungsgemeinschaft (DFG); Finanzministerium Baden-Württemberg; Helmholtz Alliance for Astroparticle Physics (HAP); Helmholtz-Gemeinschaft Deutscher Forschungszentren (HGF); Ministerium für Kultur und Wissenschaft des Landes Nordrhein-Westfalen; Ministerium für Wissenschaft, Forschung und Kunst des Landes Baden-Württemberg; Italy – Istituto Nazionale di Fisica Nucleare (INFN); Istituto Nazionale di Astrofisica (INAF); Ministero dell'Istruzione, dell'Universitá e della Ricerca (MIUR); CETEMPS Center of Excellence; Ministero degli Affari Esteri (MAE), ICSC Centro Nazionale di Ricerca in High Performance Computing, Big Data and Quantum Computing, funded by European Union NextGenerationEU, reference code CN_00000013;

México – Consejo Nacional de Ciencia y Tecnología (CONACYT) No. 167733; Universidad Nacional Autónoma de México (UNAM); PAPIIT DGAPA-UNAM; The Netherlands – Ministry of Education, Culture and Science; Netherlands Organisation for Scientific Research (NWO); Dutch national e-infrastructure with the support of SURF Cooperative; Poland – Ministry of Education and Science, grants No. DIR/WK/2018/11 and 2022/WK/12; National Science Centre, grants No. 2016/22/M/ST9/00198, 2016/23/B/ST9/01635, 2020/39/B/ST9/01398, and 2022/45/B/ST9/02163; Portugal – Portuguese national funds and FEDER funds within Programa Operacional Factores de Competitividade through Fundação para a Ciência e a Tecnologia (COMPETE); Romania – Ministry of Research, Innovation and Digitization, CNCS-UEFISCDI, contract no. 30N/2023 under Romanian National Core Program LAPLAS VII, grant no. PN 23 21 01 02 and project number PN-III-P1-1.1-TE-2021-0924/TE57/2022, within PNCDI III; Slovenia – Slovenian Research Agency, grants P1-0031, P1-0385, I0-0033, N1-0111; Spain – Ministerio de Economía, Industria y Competitividad (FPA2017-85114-P and PID2019-104676GB-C32), Xunta de Galicia (ED431C 2017/07), Junta de Andalucía (SOMM17/6104/UGR, P18-FR-4314) Feder Funds, RENATA Red Nacional Temática de Astropartículas (FPA2015-68783-REDT) and María de Maeztu Unit of Excellence (MDM-2016-0692); USA – Department of Energy, Contracts No. DE-AC02-07CH11359, No. DE-FR02-04ER41300, No. DE-FG02-99ER41107 and No. DE-SC0011689; National Science Foundation, Grant No. 0450696; The Grainger Foundation; Marie Curie-IRSES/EPLANET; European Particle Physics Latin American Network; and UNESCO.